DYNAMICS OF A STRONGLY NONLINEAR SPACECRAFT STRUCTURE PART II: MODAL ANALYSIS

L. Renson, J.P. Noël, and G. Kerschen

Space Structures and Systems Lab
Aerospace and Mechanical Engineering Department, University of Liège
1, Chemin des chevreuils (B52/3), 4000, Liège, Belgium
l.renson, jp.noel, g.kerschen@ulg.ac.be

ABSTRACT

The present paper investigates the dynamics of a real-life spacecraft structure possessing a strongly nonlinear component with multiple mechanical stops. A full-scale finite element model is built for gaining additional insight into the nonlinear dynamics that was observed experimentally in a companion paper [NRK14]. To this end, advanced techniques and theoretical concepts such as numerical continuation and nonlinear normal modes are exploited.

Key words: Spacecraft structure; piecewise-linear nonlinearities; numerical continuation; nonlinear normal modes; modal interactions.

1. INTRODUCTION

It is widely accepted that virtually all engineering structures are nonlinear, at least in certain regimes of motion. Even if the common industrial practice is to ignore nonlinearity, a recent trend is to exploit them for engineering design, *e.g.*, for vibration absorption and mitigation [VGB$^+$09, GAT$^+$07]. The last decade witnessed progresses in this direction, and, in particular, in the analysis of nonlinear aerospace structures. Moreover, substantial efforts were made to address the numerical modeling of complex, nonlinear aerospace structures (see, *e.g.*, [PE07]). Analysis using advanced numerical continuation techniques was also carried out in [WLZ10, KKL11].

Very few studies attempted to numerically analyze and experimentally compare the dynamics of a real-life structure in strongly nonlinear regimes of motion. This is the main contribution of the present paper. The identification of the SmallSat spacecraft, a satellite possessing a nonlinear component with multiple axial and lateral mechanical stops, was achieved in [NRK14] using measurements collected during a typical qualification test campaign. The present paper builds a full-scale computational model of the satellite for gaining additional insight into the nonlinear dynamics that was observed experimentally. To this end, advanced techniques and theoretical concepts such as numerical continuation [MFG$^+$03] and nonlinear normal modes [VMM$^+$08, KPGV09] are exploited. We note that a formal model updating process could not be achieved during the test campaign. Bringing the predictions of the model in close quantitative agreement with the experimental results is therefore not the objective of this paper.

The paper is organized as follows. A detailed finite element model of the underlying linear satellite is first built in Section 2 and reduced using the Craig-Bampton technique. The model identified experimentally for the nonlinear vibration isolation device is presented and incorporated in the finite element model. The nonsmooth nonlinearities in the model are regularized for facilitating the ensuing numerical simulations. Section 3 carries out a nonlinear modal analysis of the SmallSat spacecraft. It discusses in great detail the behavior of two normal modes exhibiting nonlinear interactions. The conclusions of this study are drawn in Section 4.

2. THE SMALLSAT SPACECRAFT STRUCTURE

The SmallSat structure was conceived by EADS-Astrium as a low-cost platform for small satellites in low earth orbits. It is a monocoque, octagon tube structure which is 1.2 m in height and 1 m in width [NRK14], as shown in Fig. 1 (a). The spacecraft structure supports a dummy telescope mounted on a baseplate through a tripod. The dummy telescope plate is connected to the SmallSat top floor by three shock attenuators, termed shock attenuation systems for spacecraft and adaptor (SASSAs).

Besides, as depicted in Fig. 1 (b), a support bracket connects to one of the eight walls the so-called wheel elastomer mounting system (WEMS) which is loaded with an 8-kg dummy inertia wheel. The WEMS acts as a mechanical filter which mitigates high-frequency disturbances coming from the inertia wheel through the presence of a soft elastomeric interface between its mobile

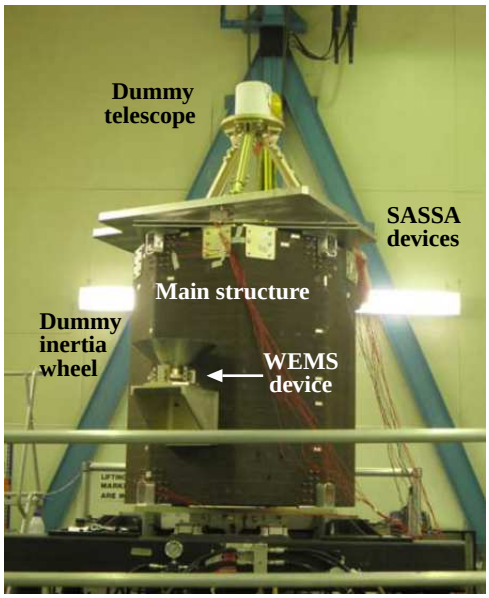

(a)

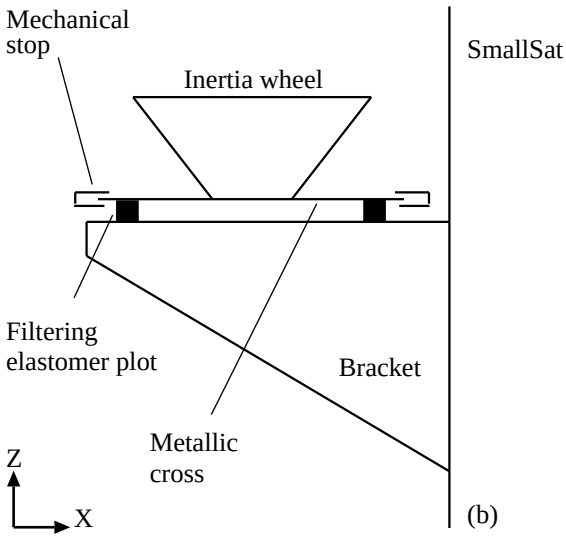

(b)

Figure 1: SmallSat spacecraft equipped with an inertia wheel supported by the WEMS and a dummy telescope connected to the main structure by the SASSA isolators. (a) Photograph; (b) schematic of the nonlinear vibration isolation device.

part, *i.e.* the inertia wheel and a supporting metallic cross, and its fixed part, *i.e* the bracket and by extension the spacecraft. Moreover, the WEMS incorporates eight mechanical stops, covered with a thin layer of elastomer, and designed to limit the axial and lateral motions of the inertia wheel during launch, which gives rise to strongly nonlinear dynamical phenomena (cf. Section 2.3).

2.1. Finite element modeling of the underlying linear satellite

A finite element model (FEM) of the SmallSat satellite created in the LMS-SAMTECH SAMCEF software is used in the present study to conduct numerical experiments. It comprises about 150,000 degrees of freedom (DOFs). The model idealizes the composite tube structure using orthotropic shell elements. The top floor, the bracket, and the wheel support are also modeled using shell elements. Boundary conditions are enforced at the base of the satellite through 4 clamped nodes. Proportional damping using the parameters provided by EADS-Astrium is also introduced in the model.

The typical frequency range of interest for spacecraft testing is between 5 and 100 Hz. Within this frequency interval, the model comprises 18 linear normal modes (LNMs) that can be classified into three groups of six modes, as listed in Table 1. The first group, between 8 Hz and 29 Hz, shows local WEMS motions. Modes 1 and 2 consist in a concave trajectory of the WEMS about Y and X axes, respectively. Modes 3 and 5 correspond to a convex trajectory of the WEMS about Y and X axes, respectively. The fourth mode presents an in-plane rotation and extension of the WEMS cross. Only mode 6 combines a significant bracket deflection with a vertical WEMS motion. The deformed shapes of modes 1 and 6 are depicted in Fig. 2. The second group, between 32 and 58 Hz, is composed of local SASSA modes including global deformation of the main structure. The last group comprises modes with local deformation of the main structure panels often combined with bracket deformation.

Mode	Model freq. [Hz]	Experimental freq. [Hz]
1	8.06	8.19
2	9.14	–
3	20.44	–
4	21.59	–
5	22.05	20.18
6	28.75	22.45
7	32.49	–
8	34.78	34.30
9	39.07	–
10	40.78	43.16
11	45.78	45.99
12	57.76	55.71
13	68.99	64.60
14	75.14	–
15	79.82	–
16	83.36	–
17	89.01	88.24
18	95.30	–

Table 1: Comparison between numerical and experimental natural frequencies. A dash means that the corresponding mode could not be identified during the test campaign.

Low-level random data acquired during the test campaign were used in the companion paper [NRK14] to extract the

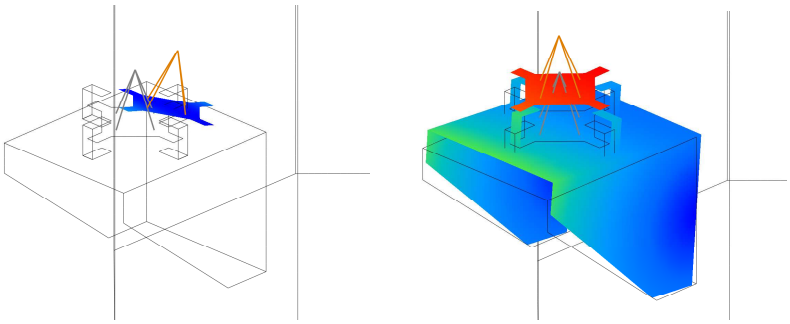

(a) (b)

Figure 2: Close-up of the (a) first LNM and (b) sixth LNM (local WEMS motion).

modal parameters of the underlying linear satellite. As stressed in the introductory section of the present paper, a formal model updating process could not be achieved during the test campaign. Nonetheless, the good agreement in Table 1 between the natural frequencies predicted by the FEM and those identified experimentally together with the correct mode ordering confirm that the model should have satisfactory predictive capabilities.

2.2. Reduced-order modeling

Because the WEMS nonlinearities are spatially localized, condensation of the linear FEM can be effectively achieved using the Craig-Bampton reduction technique [BC68]. This leads to a substantial decrease in the computational burden without degrading the accuracy of the numerical simulations in the frequency range of interest. The Craig-Bampton method expresses the complete set of initial DOFs in terms of retained DOFs and internal vibration modes of the structure clamped on the retained nodes. To introduce the WEMS nonlinearities, the reduced-order model (ROM) is constructed by keeping one node on both sides of the lateral and axial mechanical stops. In total, eight nodes of the initial FEM possessing 3 DOFs each and 10 internal modes of vibration are kept; this reduced model possesses 34 DOFs and is termed ROM810.

The ROM accuracy is assessed by comparing its modal parameters with those of the original full-scale model. The deviation between the mode shapes is determined using the modal assurance criterion (MAC). MAC value ranges from 0 in the absence of correlation to 1 for a complete correspondence. A very good correlation for the first 18 modes which cover the frequency range of interest is obtained as the frequency and MAC deviations are both below 1 $\%$.

2.3. Modeling of the WEMS nonlinearities

Fig. 3 (a) presents a simplified, yet relevant, modeling of the WEMS where the inertia wheel, owing to its important rigidity, is seen as a point mass. The four nonlinear connections (NCs) between the WEMS mobile and fixed parts are labeled NC 1 – 4, respectively.

The WEMS nonlinearities were accurately identified in the first part [NRK14] of this two-part study using data measured under swept-sine base excitations at different amplitude levels. For instance, the stiffness curve characterizing NC 1 is depicted in Fig. 3 (b). It turns out from this figure that the WEMS modeling should account for combined nonsmooth and gravity-induced asymmetric effects. This leads us to select a trilinear model k_-, k and k_+ with dissimilar clearances a_- and a_+ for the axial nonlinearities. For the lateral nonlinearities, a bilinear model $k_\pm$ and k suffices, because there is only one clearance $a_\pm$ per connection. The estimation of the stiffness and clearance parameters is detailed in the companion paper [NRK14].

Finally, for facilitating the numerical investigations in the forthcoming sections, the continuity of the first derivative of the different restoring forces of the WEMS is enforced using regularization. This approach is also motivated by the stiffness curve in Fig. 3 (b), which reveals that the actual structural behavior is smoother than a piecewise-linear law. A local regularization using Hermite polynomials in the interval $[a-\Delta, a+\Delta]$ is considered where a and 2Δ are the clearance and the size of the regularization interval, respectively. The nominal interval considered throughout the paper is equal to 5% of the clearance size.

3. NONLINEAR MODAL ANALYSIS OF THE SMALLSAT SPACECRAFT

The damped dynamics of a nonlinear system can be interpreted based on the topological structure and the bifurcations of the nonlinear normal modes (NNMs) of the

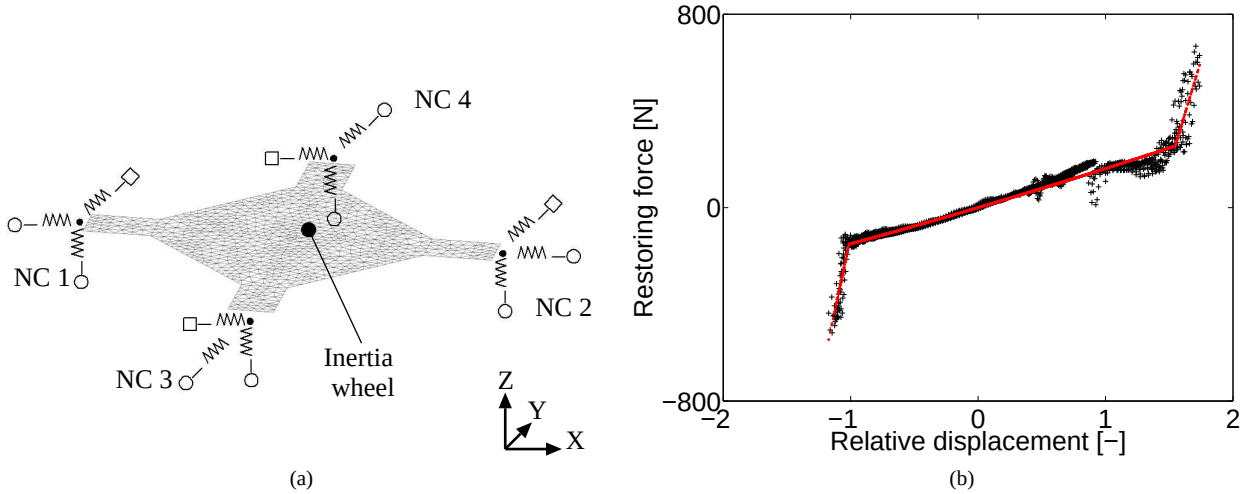

(a) (b)

Figure 3: WEMS device. (a) Simplified modeling of the WEMS mobile part considering the inertia wheel as a point mass. The linear and nonlinear connections between the WEMS mobile and fixed parts are signaled by squares and circles, respectively. (b) Experimental stiffness curve of NC 1 (in black) and fitted trilinear model (in red).

underlying conservative system [KPGV09]. A detailed nonlinear modal analysis is thus carried out herein to investigate the nonlinear phenomena observed during the testing campaign.

An extension of Rosenberg's definition is considered, *i.e.*, an NNM is defined as a (nonnecessarily synchronous) periodic motion of the unforced, conservative system. The algorithm proposed in [PVS$^+$09], which combines shooting and pseudo-arclength continuation, is applied to the ROM810 model for NNM computation. Due to the frequency-energy dependence of nonlinear oscillations, NNMs are depicted in a frequency-energy plot (FEP). An NNM is represented by a point in the FEP, drawn at a frequency corresponding to the minimal period of the periodic motion, and at an energy equal to the conserved total energy during the motion. A branch depicted by a solid line represents the complete frequency-energy dependence of the considered mode.

The first linear normal mode (LNM1) corresponds to a local motion involving the WEMS. Its nonlinear counterpart is pictured in Fig. 4. The FEP of NNM1 is formed by one main backbone to which one "tongue" is attached. At low energies, no mechanical stop is activated, and the NNM frequency remains identical to the natural frequency of LNM1. The corresponding modal shape is also identical to that of LNM1. Beyond a certain energy threshold, the relative displacements along X of nonlinear connections NC 1 and NC 2 enter into the regularization area of the piecewise-linear restoring forces. The NNM frequency rapidly increases due to the large difference between the stiffnesses of the elastomer plots and of the mechanical stops. When progressing along the backbone, harmonic components of the fundamental NNM oscillation frequency are created by the WEMS nonlinearities. Once one of these harmonics has a frequency close to the oscillation frequency of another NNM, a dynamic coupling between the two modes exists, and a tongue of internal resonance is produced. This is precisely what happens for the 5:1 internal resonance in Fig. 4. As energy increases along this branch, the fifth harmonic becomes more important than the fundamental frequency. The modal shape located around the middle of the branch is a mixing between NNM1 and NNM10; it is a purely nonlinear mode with no linear counterpart. At the extremity, the sole fifth harmonic remains, which completes the transition to NNM10. Such internal resonances between NNMs were previously reported in the literature, see, *e.g.*, [KPGV09, LKV$^+$05], and also in the case of a full-scale aircraft [KPGS12]. They are therefore not further described herein. However, it is interesting to note that, due to nonlinearities, the excitation of a local mode, *i.e.* NNM1, can trigger the excitation of a more global mode, *i.e.* NNM10, involving instrument panel motion. This latter mode is characterized by a much larger modal mass and can potentially jeopardize the structural integrity during launch.

A second local mode of the WEMS, NNM6, is presented in Fig. 5. A 2:1 modal interaction during which NNM6 interacts with NNM12 is found to exist. NNM12 corresponds to an axial motion of the instrument supporting panel. Numerical evidence of this interaction is provided by analyzing the response at the instrument panel to swept-sine excitation in Fig. 6 (a). Damping is included in the numerical simulation. For a forcing amplitude of 20 N, the satellite presents several resonance peaks at frequencies equal to the linear natural frequencies (see Table 1). For a forcing amplitude of 80 N, an additional resonance peak corresponding to an excitation frequency of 29 Hz can be observed. The presence of this resonance cannot be predicted by a linear analysis, because there is no linear mode possessing instrument panel motion below 32 Hz. It is therefore a nonlinear resonance during

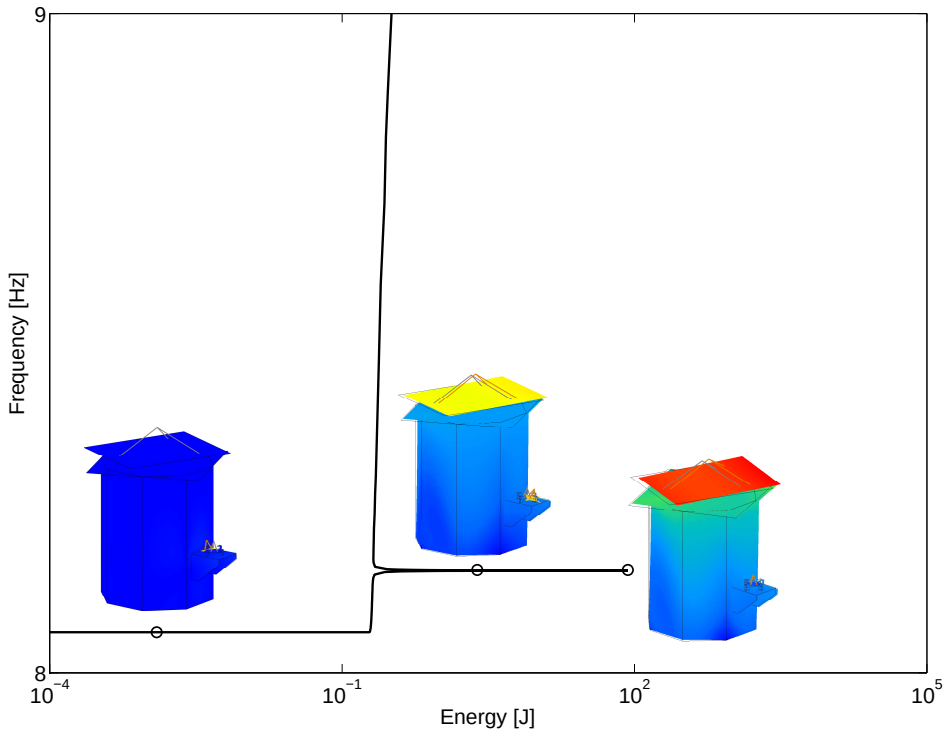

Figure 4: FEP of the first NNM with different modal shapes inset.

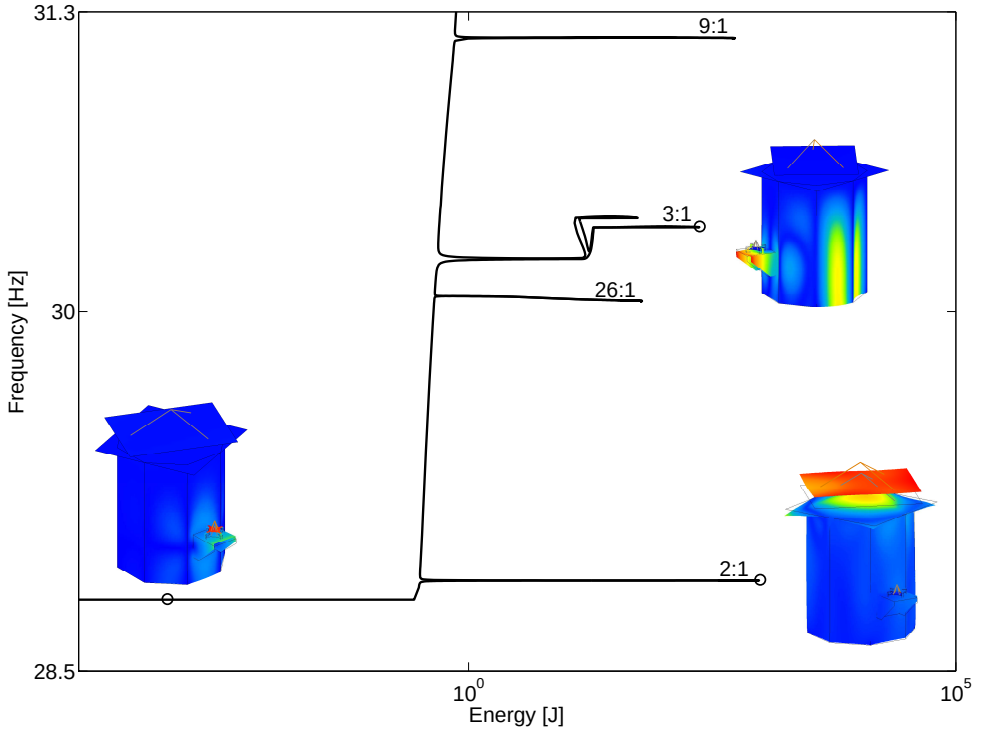

Figure 5: FEP of the sixth NNM with different modal shapes inset.

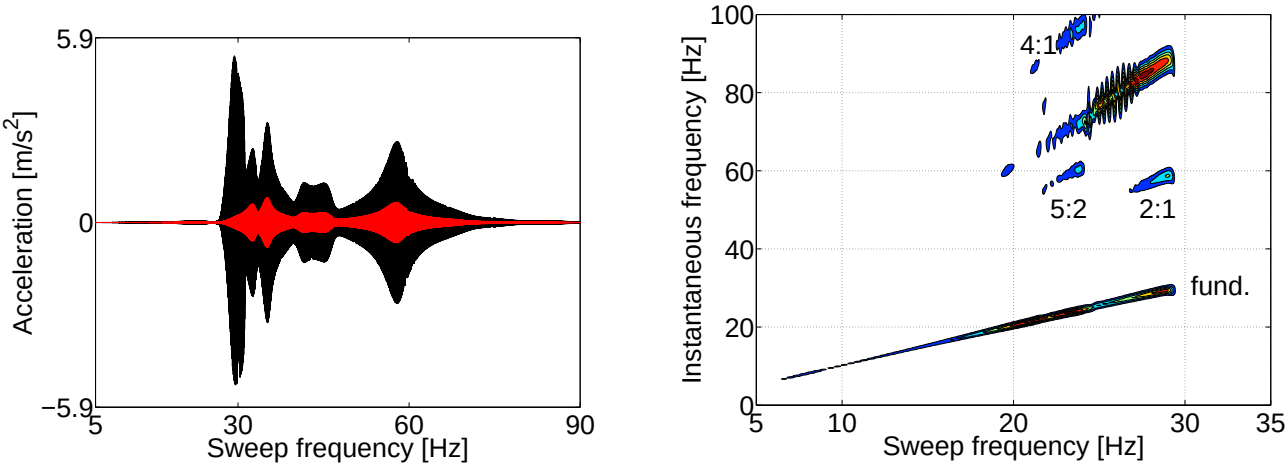

Figure 6: Numerical and experimental evidence of the 2:1 modal interaction between NNM6 and NNM12. (a) Acceleration at the instrument panel for a swept-sine excitation of 20 N (red) and 80 N (black) amplitude (direct numerical simulation); (b) wavelet transform of the relative displacement at NC 4 – Z (measured during the testing campaign).

which the second harmonic of NNM6 characterized by a frequency close to 58 Hz excites NNM12. This, in turn, produces a large response at the instrument panel when the excitation frequency is in the vicinity of NNM6. Interestingly, this nonlinear resonance has an acceleration twice as large as the acceleration corresponding to the linear resonance of the panel at 58 Hz. Further experimental evidence of the modal interaction is shown in the wavelet transform measured at NC 4 in Fig. 6 (b) [NRK14]. The excitation frequency, denoted by fund., is accompanied with higher harmonic components of comparable amplitudes. Specifically, a second harmonic ranging from 55 to 60 Hz is visible when the excitation frequency approaches 30 Hz. There is no identified linear mode just below 30 Hz, but, due to the hardening effect of the WEMS, the linear frequency of 22.45 Hz increases substantially during nonlinear regimes of motion. The second harmonic then excites the experimental mode with a linear frequency of 55.71 Hz.

4. CONCLUSION

The objective of this paper was to investigate the dynamics of a real-life spacecraft structure with a strongly nonlinear component. Due to the presence of multiple nonsmooth nonlinearities, closely-spaced modes and relatively high damping, this application example poses several challenges. One specific contribution of this work is that one interaction between nonlinear modes with noncommensurable linear frequencies, observed experimentally, was reproduced with great fidelity using numerical experiments. Note that additional nonlinear phenomena the SmallSat spacecraft may exhibit, including jumps, rich frequency content, quasiperiodic motion, internal resonance branches with nonconventional topology and mode localization, are analyzed in [RNK14].

The present paper and its companion [NRK14] demonstrate that there now exist in the technical literature effective and rigorous numerical and experimental methods for the analysis of complex, nonlinear industrial structures.

ACKNOWLEDGMENTS

This paper was prepared in the framework of the European Space Agency (ESA) Technology Research Programme study “Advancement of Mechanical Verification Methods for Non-linear Spacecraft Structures (NOLISS)” (ESA contract No.21359/08/NL/SFe). Experimental data were measured by EADS-Astrium and LMS International. The authors also thank Astrium SAS for sharing information about the SmallSat spacecraft. The authors L. Renson and J.P. Noël are Research Fellows (FRIA fellowship) of the *Fonds de la Recherche Scientifique – FNRS* which is finally gratefully acknowledged.

REFERENCES

[BC68] M. C. C. Bampton and Jr. R. R. Craig. Coupling of substructures for dynamic analyses. *AIAA Journal*, 6(7):1313–1319, 1968.

[GAT+07] E. Gourdon, N. A. Alexander, C. A. Taylor, C. H. Lamarque, and S. Pernot. Nonlinear energy pumping under transient forcing with strongly nonlinear coupling: Theoretical and experimental results. *Journal*

of Sound and Vibration, 300(3-5):522–551, 2007.

[KKL11] J. A. C. Knowles, B. Krauskopf, and M. H. Lowenberg. Numerical continuation applied to landing gear mechanism analysis. *Journal of Aircraft*, 48:1254–1262, 2011.

[KPGS12] G. Kerschen, M. Peeters, J.C. Golinval, and C. Stephan. Nonlinear normal modes of a full-scale aircraft. *AIAA Journal of Aircraft, in press*, 2012.

[KPGV09] G. Kerschen, M. Peeters, J. C. Golinval, and A. F. Vakakis. Nonlinear normal modes, Part I: A useful framework for the structural dynamicist. *Mechanical Systems and Signal Processing*, 23(1):170–194, 2009.

[LKV+05] Y. S. Lee, G. Kerschen, A. F. Vakakis, P. Panagopoulos, L. Bergman, and D. M. McFarland. Complicated dynamics of a linear oscillator with a light, essentially nonlinear attachment. *Physica D: Nonlinear Phenomena*, 204(1-2):41–69, 2005.

[MFG+03] F.J. Muñoz-Almaraz, E. Freire, J. Galán, E. Doedel, and A. Vanderbauwhede. Continuation of periodic orbits in conservative and hamiltonian systems. *Physica D: Nonlinear Phenomena*, 181(1-2):1–38, 2003.

[NRK14] J.P. Noël, L. Renson, and G. Kerschen. Dynamics of a strongly nonlinear spacecraft structure. Part I: Experimental identification. In *Proc. of the Eur. Conf. on Spacecraft Structures, Materials and Environmental Testing*, Braunschweig, Germany, 2014.

[PE07] E. P. Petrov and D. J. Ewins. Advanced modeling of underplatform dampers for analysis of bladed disk vibration. *Journal of Turbomachinery*, 129:143–150, 2007.

[PVS+09] M. Peeters, R. Viguié, G. Sérandour, G. Kerschen, and J. C. Golinval. Nonlinear normal modes. Part II: Toward a practical computation using numerical continuation techniques. *Mechanical Systems and Signal Processing*, 23(1):195–216, 2009.

[RNK14] L. Renson, J.P. Noël, and G. Kerschen. Complex dynamics of a nonlinear aerospace structure: Numerical continuation and normal modes. *Nonlinear Dynamics*, in review, 2014.

[VGB+09] A. F. Vakakis, O. Gendelman, L. A. Bergman, D. M. McFarland, G. Kerschen, and Y. S. Lee. *Nonlinear Targeted Energy Transfer in Mechanical and Structural Systems*. Springer, Series: Solid Mechanics and Its Applications, Vol. 156, 2009.

[VMM+08] A. F. Vakakis, L. I. Manevitch, Y. V. Mlkhlin, V. N. Pilipchuk, and A. A. Zevin. *Normal Modes and Localization in Nonlinear Systems*. Wiley-VCH Verlag GmbH, 2008.

[WLZ10] F. Wei, L. Liang, and G. T. Zheng. Parametric study for dynamics of spacecraft with local nonlinearities. *AIAA Journal*, 48:1700–1707, 2010.